Experimental comparisons between one-part and normal (two-part) alkali-activated slag binders

Ren, Jie; Sun, Hongfang ; Li, Qun ; Li, Zhenming; Ling, Li ; Zhang, Xiaogang ; Wang, Yanshuai ; Xing, Feng

DOI
10.1016/j.conbuildmat.2021.125177

Publication date
2021

Document Version
Accepted author manuscript

Published in
Construction and Building Materials

Citation (APA)
Ren, J., Sun, H., Li, Q., Li, Z., Ling, L., Zhang, X., Wang, Y., & Xing, F. (2021). Experimental comparisons between one-part and normal (two-part) alkali-activated slag binders. *Construction and Building Materials*, *309*, 1-10. Article 125177. https://doi.org/10.1016/j.conbuildmat.2021.125177

Experimental comparisons between one-part and normal (two-part) alkali-activated slag binders

Jie Ren[1,*], Hongfang Sun[1], Qun Li[1], Zhenming Li[2,*], Li Ling[1], Xiaogang Zhang[1], Yanshuai Wang[1], Feng Xing[1]

[1] Guangdong Provincial Key Laboratory of Durability for Marine Civil Engineering, College of Civil and Transportation Engineering, Shenzhen University, Shenzhen 518060, China

[2] Department of Materials, Mechanics, Management & Design, Faculty of Civil Engineering and Geoscience, Delft University of Technology, Delft, the Netherlands

*Corresponding authors.

Abstract

One-part alkali-activated slag (AAS) binders are more promising in large-scale constructions because one-part mixing procedure is safer and easier to handle compared to normal two-part method. Thus, this study aims at investigating different properties of one-part AAS binders and control samples prepared using the two-part method. Experimental results of the former suggested the hardening time was greatly extended, but the workability showed little difference. Besides, compared to the control, one-part AAS binders had similar early compressive strength (within 7 days) and flexural strength in all tested curing stages but lower later compressive strength (from 28 days). The characterisation of the porous structures suggests that there were fewer C-A-S-H gels for one-part binders evidenced by less volume of mesopores but with larger amount of bigger pores. In addition, mineralogical and microstructural analyses imply that there was no hydrotalcite formed in the one-part AAS binders. Moreover, one-part AAS binders are more susceptible to efflorescence, presumably further affecting their surface and long-term durability.

Key words: One-part alkali-activated slag; Mechanical properties; Mineralogical and microstructural analysis; Pore microstructure; Efflorescence

1. Introduction

Traditional ordinary Portland cement (OPC) manufacturing is a major contributor to the global carbon dioxide emissions due to massive amount of CO_2 released from the calcination of limestone at 1400-1450 ℃ and corresponding intensive energy consumption involved. For instance, in 2016, the total CO_2 emission caused by the manufacturing of OPC was around 1.45

Gt, which was approximately 8% of the total anthropogenic CO_2 emissions [1]. Thus, many researchers are seeking for alternative binders with low-carbon footprint [2-8]. Alkali-activated slag (AAS) requires no heat curing and has a relatively higher early strength, low permeability and stronger thermal stability as well as durability compared to OPC-based binders [4, 9-13]. However, the commonly-seen traditional activation process of AAS, also considered as two-part mixing, involves preparation of concentrated alkaline solutions which are quite corrosive and viscous, such as sodium (or potassium) hydroxide in particular. This is especially inconvenient and unsafe for cast-in-situ large-scale applications.

One-part (also known as 'just add water') AAS binders are now gaining an increasing attention from both academia and industrial sectors because they provide a safer and easier-to-handle approach for wider applications of AAS binders compared to traditional two-part AAS counterparts [14-17]. One-part AAS binders are prepared by simply adding water into a mixture of slag, various types of solid activators and aggregates, similar to the preparation of OPC-based binders. Apart from the advantages including safety and easy-to-handle approach, one more advantage of using one-part mixing method for AAS binders is that it could to some extent counteract the weakness of low-temperature mixing and curing such as subzero-temperature concreting because low temperature could retard the hardening reactions of alkali-activated materials [18, 19]. Specifically, when in contact with water, solid activators such as sodium silicate or sodium hydroxide particles would release a large amount of heat, increasing the temperature of whole mixtures. A few researches have already explored the viability of one-part mixing method and corresponding properties of one-part AAS binders [14, 17, 20, 21]. Alzaza et al. [21] investigated the effects of low-temperature curing on the hardened properties of one-part AAS and OPC-based binders. The results showed that although a lower curing temperature would result in greater reduction in the compressive strength of mortars, the one-part AAS binders achieved higher compressive strength compared to OPC-based counterparts. Besides, after an extra room-temperature curing regime, the hardened properties of AAS could be improved significantly. According to another study [14], the initial mixing water temperature would influence the dissolution rate of solid activators. The experimental work conducted by Luukkonen et al. [20] highlighted the importance of silica availability in determining the fresh and hardened properties of one-part AAS binders. Despite of these research, there is still some debate regarding various properties of AAS binders such as compressive strength [22, 23], which might be due to a lack of systematic and comprehensive investigation.

This study investigates the fresh and hardened properties of a type of one-part AAS binders, including setting time, fluidity, hydration heat evolution, mechanical properties accompanied with pore-related microstructures and mineralogical/microstructural characteristics. Reference binders prepared with the same mixture proportion but using the normal (two-part) mixing method were also made. The outcomes from this research are expected to enhance the technical feasibility and commercial viability of AAS binders in related industries, especially for future constructions in cold regions and countries.

2. Experimental programme

2.1. Raw materials

The slag used in this study was granulated blast furnace slag (hereafter referred to as GBFS), provided by Wuhan SinoCem Smartec Co., Ltd. Its specific density and Blaine fineness was 2900 kg/m^3 and 424 m^2/kg, respectively. The d_{10}, d_{50} and d_{90} of the GBFS used was 2.0, 12.5 and 38.4 μm accordingly with its particle size distribution and morphology shown in Fig. 1(a) and (b). The chemical composition of GBFS is tabulated in Table 1. Anhydrous sodium metasilicate (Na_2SiO_3) fine powders were employed as the solid activator with SiO_2/Na_2O molar ratio at 1:1. Standard river sand was used as the fine aggregate for mortar specimens, in accordance with GB/T 14684, which was supplied by Xiamen ISO Standard Sand Co., Ltd (Xiamen, China). Distilled water was used as the mixing water and a constant water-to-binder (GBFS) ratio of 0.40 was fixed for the two different mixtures.

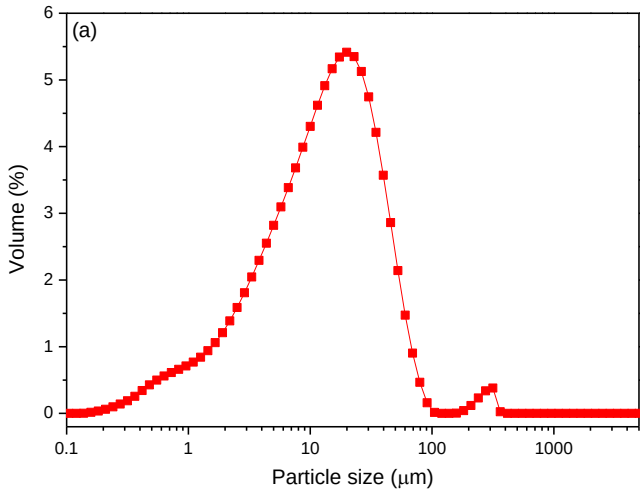

(b)

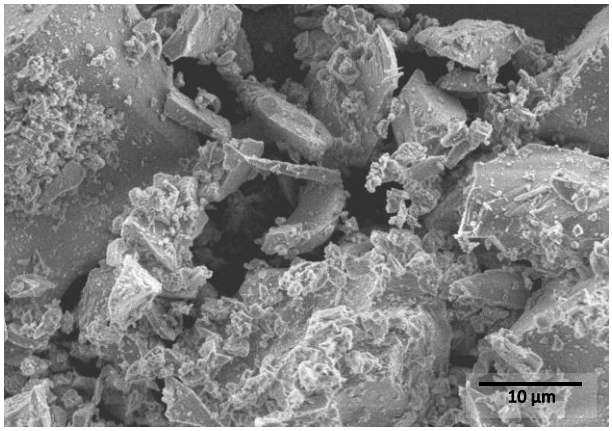

Fig. 1. Particle size distribution (a) and the morphology of the GBFS (b) used in this study.

Table 1

Chemical composition of the GBFS determined by X-ray fluorescence (wt.%).

Oxides	SiO_2	CaO	Al_2O_3	Fe_2O_3	Na_2O	K_2O	MgO	TiO_2	MnO	SO_3	Others	LOI
Content	31.86	39.81	16.53	0.43	0.33	0.54	6.89	1.23	0.18	0.04	2.14	0.02

LOI is loss on ignition at 1000 ℃.

2.2. Sample preparation

For the normal two-part AAS binders, the alkali-activator solution was prepared by mixing the solid sodium metasilicate fine particles with distilled water first using a magnetic stirrer and cooled off in ambient environment until reaching room temperature (23 ± 2 ℃). GBFS (for pastes) or GBFS and sand (for mortars) were dry mixed for 2 min followed by adding the activator into the dry mixture with a continued mixing for 7 min prior to further procedures. For the one-part mixing, sodium metasilicate particles were directly added into the mixing bowl with pre-weighed GBFS (for pastes) and sand (for mortars), as shown in Fig. 2. Then these raw materials were dry mixed for 2 min, and the mixing water at room temperature was gradually poured with a further mixing for 7 min at low speed. After mixing, newly-mixed specimens were cast into different moulds, vibrated on a vibrating table for 30 seconds to remove air bubbles. For mortars, a part of them was used for fluidity test based on the mini-slump test. For paste slurries, they were used for setting time measurement and mineralogical as well as hydration kinetic analysis. The samples in different moulds were covered with plastic films in order to minimise moisture loss at room temperature (23 ± 2 ℃) and demoulded after one day, sealed tightly in plastic bags in an ambient environment (23 ± 2 ℃, RH = 50 ± 5%) for different ages prior to further tests. The dosage of the solid activator powder was 7% by mass of the

GBFS and the sand-to-binder ratio was 2.0 for preparing mortar specimens. The detailed mix proportion was determined based on our pre-tests [11, 24, 25].

Fig. 2. Direct addition of sodium metasilicate particles into the dry mixture (GBFS + sand) prior to the addition of distilled water into the system.

The temperature of the mortar specimen while mixing was measured every two minutes right after the addition of the distilled water or the alkaline activator solution, which is also known as wetting point (liquid comes into contact with solid materials). The corresponding value was 29.6 ℃, 28.8 ℃ and 29.0 ℃ after 2, 4, 6 minutes of mixing for the one-part mortar specimens. In comparison, for the normal specimens, the corresponding value was 23.5, 25.3 and 25.5 ℃, respectively. The averaged value of the three readings was 29.1 ℃ and 24.8 ℃ for the one-part and normal AAS mortars accordingly. The detailed temperature changes over the mixing procedure are also shown in Fig. 3. Therefore, it is apparent that one-part AAS binders had a higher temperature while mixing due to the activator powder dissolution into water. The higher temperature of mixing water could increase the mixture temperature, which may lead to quicker water loss. A quicker water loss may then result in a higher concentration of alkalis with an expected rise in pH value for those sodium metasilicate fine powders that were already dissolved in the water solution [26]. A schematic presentation of the two different mixing procedures, namely one-part and normal (two-part) methods, is described in Fig. 4.

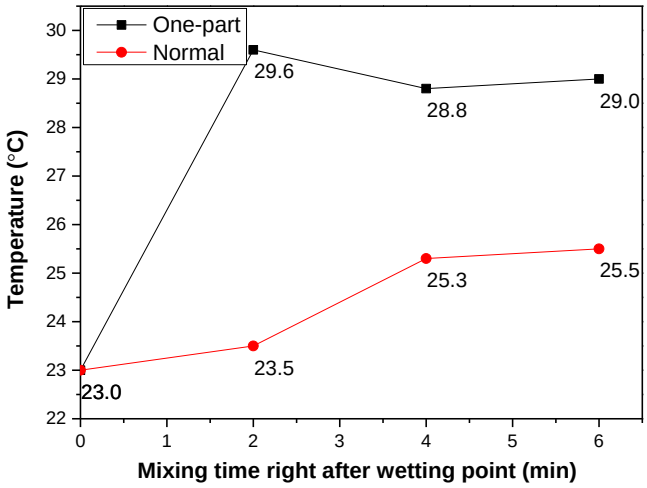

129

130 **Fig. 3.** Temperature changes during the mixing procedure for one-part and the normal AAS

131 paste specimens.

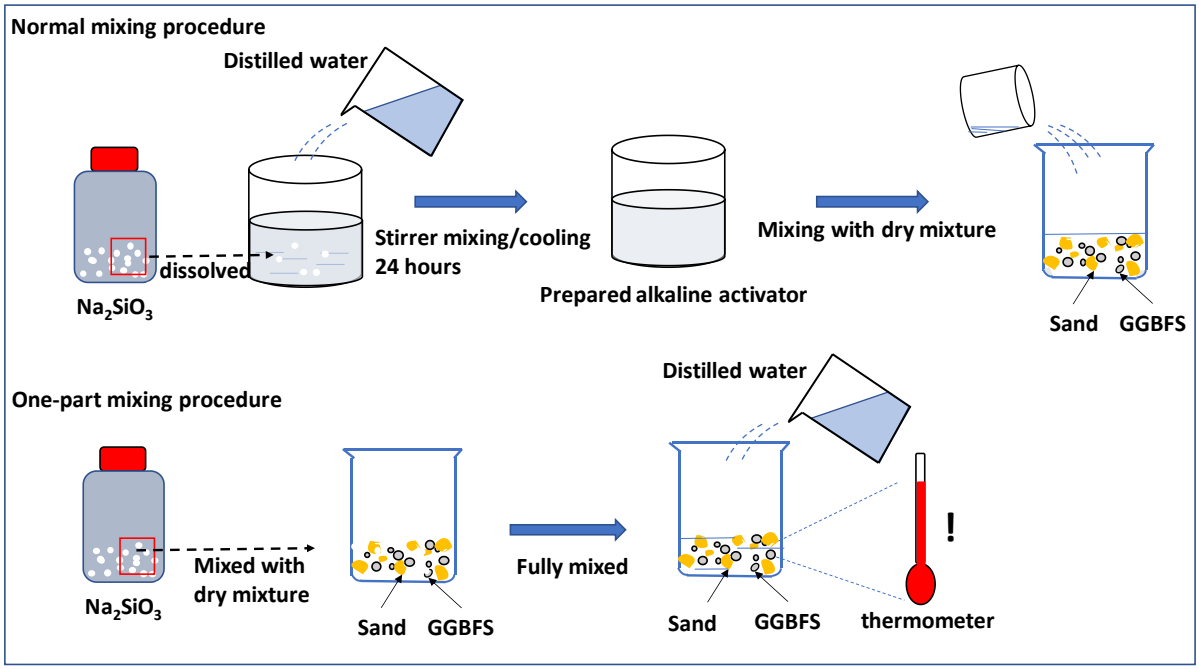

132

133 **Fig. 4.** Schematic presentation of the two mixing methods, namely one-part and normal

134 mixing procedures (two-part) for the AAS mortar specimens.

135

136 ## 2.3. Test procedures

137 ### 2.3.1. Setting time, fluidity and calorimetric analysis

138 Setting time including initial and final setting time was measured using a Vicat needle based

139 on ASTM C191-19.

Fluidity was evaluated using mini slump test, in accordance with ASTM C1437-15. The results were expressed as the averaged values of two perpendicular measurements of the spread diameter for mortar binders.

For heat evolution measurement based on calorimetric analysis, the heat flow soon after achieving the wetting point for paste slurries was captured inside an isothermal calorimeter. Specifically, around 7 g slurries for the two types of pastes were filled into a glass ampoule and securely sealed, followed by immediately placing into the isothermal calorimeter (TAM AIR). The heat profiles over the following 96 hours were carefully monitored.

2.3.2. Mechanical strength and pore-related properties

The compressive strength and flexural strength in three-point bending mode was measured to assess the mechanical properties of the one-part and normal AAS mortar specimens after different curing ages. Prismatic samples sizing at 40 mm × 40 mm × 160 mm and cubic ones with a dimension of 40 mm × 40 mm × 40 mm were used for flexural strength and compressive strength, respectively. The loading rate was 2.4 kN/s for compressive strength and 50 N/s for flexural strength measurement. The compressive strength was measured at the age of 1 day, 7 days, 28 days, 56 days and 90 days. Since the two mixtures showed rather similar compressive strength in the first 7 days, the flexural strength was measured only after 7 days. Each test was conducted in triplicates in accordance with ASTM C109M and the final results were the average values of the three readings.

Pore-related properties, including water absorption and volume of permeable voids (VPV), were measured in accordance to ASTM C642-06 after 28 and 56 days of curing. Samples were first dried at 60 ℃ in a vacuum oven until constant masses were obtained (the two consecutive measurements between a 24-hour interval was less than 0.5%). This drying temperature is different from that suggested by ASTM C642-06, due to the potential damages caused by higher temperatures on the porous microstructures of alkali-activated binders [27], as previously used in other studies [5, 25].

Besides, the total porosity and pore-size distributions of the two types of mortar mixes after 56 days of curing were estimated based on nitrogen sorption test using a surface area and porosity analyser (TriStar). Small fragments of untested specimens with sizes approximately at 5 mm were used [28] and they were vacuum dried first at 60 ℃ for at least two days and then degassed at 60 ℃ for at least 7 hours, considering many fine pores inside alkali-activated slag binding systems [11, 29]. The relative pressure was 0.053-0.993 and the isotherms were obtained based on Barrett-Joyner-Halenda (BJH) models. The similar sizes of the samples

selected were to ensure the sand in mortar specimens had no significant impact on the final results.

2.3.3. Mineralogical and microstructural analysis

X-ray diffraction (XRD) and thermogravimetric analysis (TGA) as well as differential thermogravimetry (DTG) analysis after 56 days of curing were carried out to provide information on mineralogical characteristics of the paste specimens. Paste samples were first finely grinded into powders (passing through 75 μm sieve) and dried at 50 ℃ prior to tests. For XRD test, a scanning range of 5-70° (2θ) with 0.5s/step (3183 steps in total) and a tube setting of 40 kV and 40 mA were applied using a Bruker D8 Advance diffractometer. For TGA/DTG, the test was performed using a thermal analyser (NETZSCH-STA 409 PG/PC) with the samples heated from room temperature to 1000 ℃ in a nitrogen environment.

Scanning electron microscope (SEM) in conjunction with energy dispersive spectroscopy (EDS) test was conducted on fractured paste and mortar specimens after certain curing ages using a Quanta FEG 250 high resolution scanning electron microscope device. Samples after the corresponding curing ages were first immersed in acetone solution to stop the hydration and then dried in a vacuum oven at 50 ℃ for several days before the test. Finally, they were mounted on a conductive adhesive and subjected to gold spraying prior to the SEM/EDS detection. Secondary electron (SE) mode was employed to observe the micromorphology of the products. The accelerated voltage used was 10.00 kV with a working distance of about 10 mm.

3. Results and discussion

3.1. Setting time, fluidity and heat flow profile

Table 2 shows the initial and final setting time of the one-part and normal AAS pastes. It is apparent that the former had a much longer initial and final setting time, 123 and 310 min respectively, compared to its normal counterpart (58 min and 82 min respectively). The much longer setting time is possibly due to a delayed dissolution of silica and alumina species, as well as the following gelation and condensation process because the sodium silicate powders were mixed with dry GBFS particles first before they were dissolved in water. At the same time, it is also highly possible that because of a more rapid heat release introduced by the contact of sodium metasilicate with water, part of GBFS particles were dissolved at a much higher rate compared to the normal mixing procedure. This partial and regional dissolution of GBFS led to higher hydration process and formation of a hard reaction shell, surrounding

GBFS particle surfaces. This would to some extent hinder the further hydration process [30]. According to the study [31], this reaction shell should be associated with the reaction among CaO (available immediately after the addition of water), soluble Si from the activator and partial Al released from the GBFS. The slower hardening rate for one-part alkali-activated blast furnace slag when using solid activator instead of the liquid one was also confirmed by Yang et al. [32] and Liu et al. [33] in which case the setting time of one-part AAS could be more than 5 hours whereas the one for normal two-part AAS is only about one hour. It is worth noting that the much greater elapsed time between initial and final setting time for one-part mixing (from 123 min to 310 min) indicates that the mixture ingredients might also have changed because of the one-part mixing procedure.

The mini-slump test results and fluidity of the two mixes are shown in Fig. 5 and Table 2, respectively. It can be seen that the one-part mixed mortar had a similar fluidity (spread-flow = 239 mm), indicating a comparable workability as that of the normal peer (235 mm). This result suggests that although the water was added with no sodium silicate dissolved, the whole one-part mixture still displayed a homogeneous fresh state without any segregation or bleeding. Besides, the different mixing temperature seems to have a marginal effect on the fluidity [24].

Table 2

Initial and final setting time as well as fluidity of the two mixes of AAS specimens.

Sample types	Setting time of paste (min)		Fluidity of mortar (mm)
	Initial setting time	Final setting time	
One-part	123	310	239
Normal	58	82	235

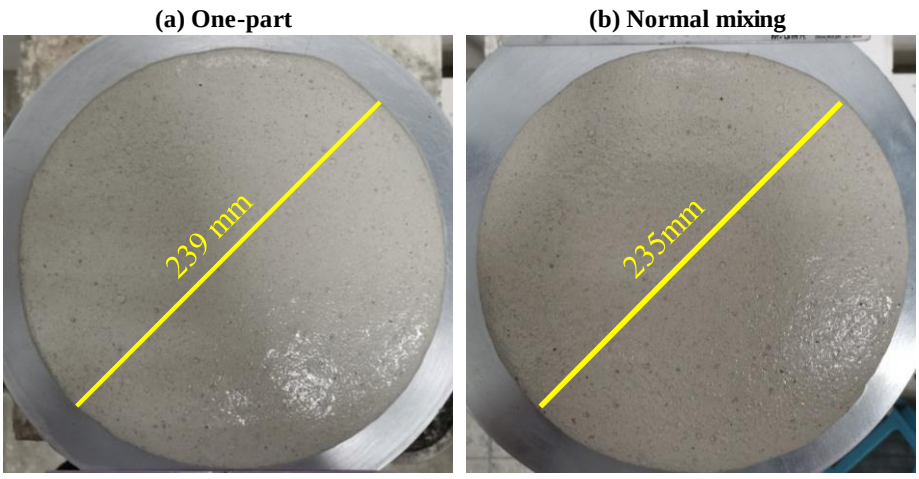

Fig. 5. Fluidity of the newly mixed AAS mortars, (a) one-part mixed paste and, (b) normal paste.

The heat flow curves of the two types AAS pastes are shown in Fig. 6. The initial peaks marked as '1' result from the wetting and dissolution of GBFS and the significantly higher peak assigned to the one-part binder should be explained by considering the heat released from the dissolution of sodium metasilicate in water, rather than the simple dissolution of GBFS in the high-alkalinity activator solution. Therefore, this peak for the one-part pastes cannot imply the actual starting point of the real hydration process. After this, a short induction period was detected followed by an acceleration stage indicated by peak '2', which is attributed to the formation of main reaction products. The starting time of the acceleration stage is marked using the dashed line 'a' and 'a'' as shown in Fig. 6. Not surprisingly, the one-part paste displayed a shorter induction period with an earlier commencement of the acceleration stage (shown as 'a'), due in large part to the partial rapid GBFS dissolution and quicker precipitation of certain reaction products on the surface of GBFS under the higher mixture temperature condition, corresponding well with other literature [14, 34]. According to the study [34], the induction period was even not detected because of the overlapping of the initial and acceleration peaks. However, the corresponding acceleration of peak '2' is obviously lower than that of the normal one. This is reasonable because some GBFS particles were covered with the hard reaction shell, impeding further reaction of GBFS particles, which is consistent with the results of setting time. This behaviour can be considered as 'premature' phenomenon, in which a regional rapid release of heat led to a seemingly faster dissolution and reaction of GBFS at the very early stage but then significantly delayed the further dissolution of GBFS particles, resulting in less heat release and much prolonged setting time. In comparison, normal AAS paste displayed a delayed acceleration stage, suggested by 'a'', but a much higher peak '2'. Related discussions on the difference between the mechanisms of setting time and acceleration period can be found in [35]. Overall, it can be concluded that the one-part mixing led to a delayed direct dissolution of GBFS into activator, but the higher mixture temperature caused by the greater amount of released heat to some extent counteracted this effect. This may further influence the mechanical strength which is discussed in the next section.

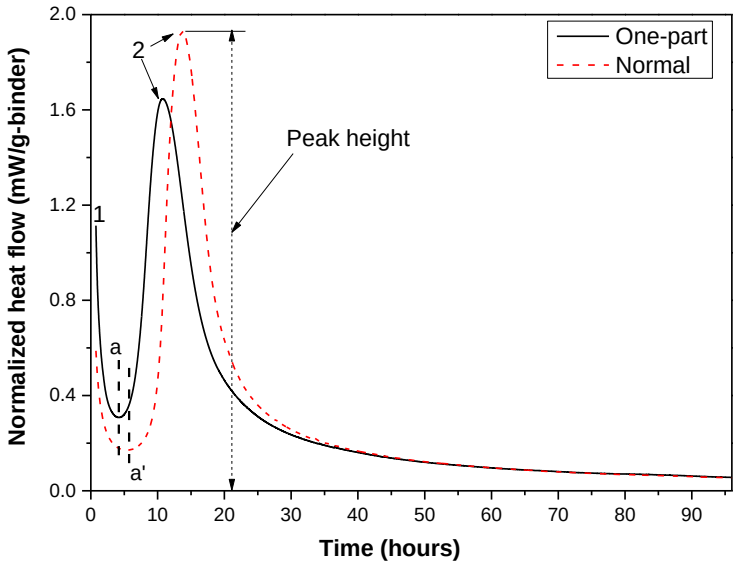

Fig. 6. Heat flow curves of the two AAS pastes over 96 hours from the addition of water (one-part) or alkaline solution (normal).

3.2. Mechanical strength and pore-related properties

Fig. 7 shows the compressive strength of the two AAS mortar mixes during 90 days of curing. It can be seen that the compressive strength increased with time for the two types of specimens. Within the 7 days of curing, there was little difference between the compressive strength of the two mortar mixes, suggesting that one-part mixing had no obvious negative impact on the early-age strength development up to around 7 days. As discussed before, during the early stages, the similar compressive strength of the two AAS mixes can be explained by considering that on the one hand, one-part mixing method led to delayed dissolution of GBFS into the alkaline activator, to some extent hindering the hydration process. One the other hand, however, the significantly increased temperature due to the contact of sodium metasilicate powders with water partially improved the solubility and diffusivity of the GBFS in the solid-liquid system [36], evidenced by the heat evolution rate as discussed earlier (Fig. 6). As a result, the latter effect counteracted the delayed development of the compressive strength. Based on these results, only the flexural strength since 28 days was measured because of the very similar compressive strength within 7 days of curing.

After that, one-part mixed mortars displayed slightly lower compressive strength compared to that of the normal mortar specimens up to 90 days of curing. For instance, the compressive strength of the one-part mixed and normal AAS mortars was about 60.4 MPa and 67.9 MPa respectively after 28 days of curing. At 90-day of curing, the corresponding value was 67.4 and 70.8 MPa. Thus, the reduction in the compressive strength for one-part mixed mortars

compared to normal peers was 11.04% and 4.83% after 28 days and 90 days, respectively. The reduced compressive strength of one-part specimens might be associated with some intrinsic defects caused by the rapid formation of hard shells around the unreacted GBFS particles because of the higher mixing temperature. Similar results were also reported from other researches [22, 37]. Besides, some carbonates or hydrogen carbonate phases formed in the highly porous and less ordered microstructure because of the insufficient reaction could also result in the degraded microstructure and hence worsened mechanical properties.

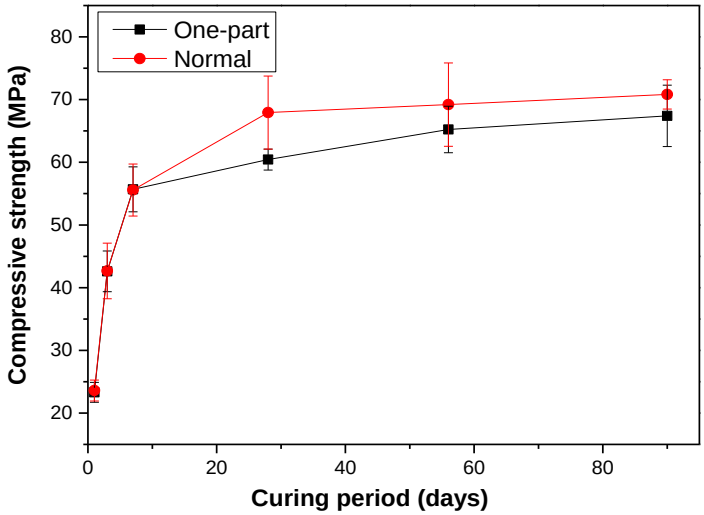

Fig. 7. Compressive strength of the one-part and normal AAS mortar specimens over 90 days of curing.

The flexural strength of the two types of mortar mixes at 28-day, 56-day and 90-day of curing is presented in Fig. 8. It is apparent that although normal specimens achieved slightly higher flexural strength values for all the testing ages, the difference between the two mortar mixes was negligible, especially considering the standard deviations for the one-part specimens. After 56 days of curing, for example, the flexural strength of the one-part specimen was only about 2.8% less than that of the normal one. These results imply that one-part mixing had no significant impact on the flexural strength of the AAS mortars.

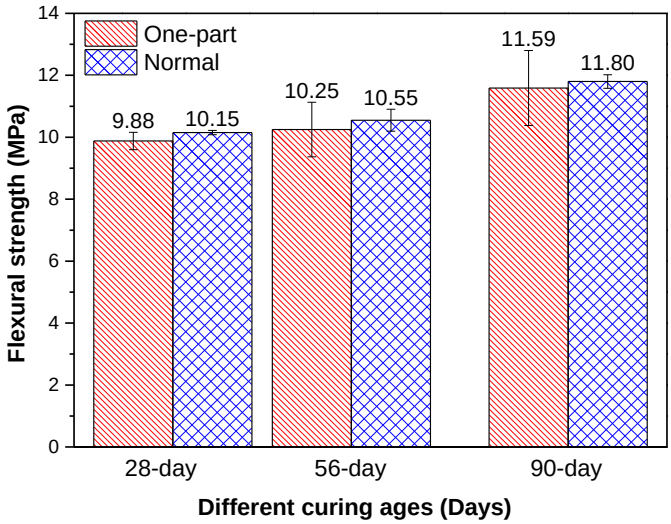

Fig. 8. Flexural strength of the one-part and normal AAS mortar specimens at 28, 56 and 90 days of curing.

Fig. 9 shows the water absorption and volume of permeable voids (VPV) of the one-part and normal AAS mortar specimens after 28 and 56 days of curing. It can be seen that the water absorption and VPV decreased as the curing time increased from 28 days to 56 days, regardless of mortar mixes [38]. Besides, after 28 days of curing, the water absorption and VPV was 3.94% and 7.34% respectively for the one-part mortar specimens, whereas the corresponding values for the normal mortar was 4.19% and 7.71%. The values for the one-part mortar were similar to the data obtained in another literature [39]. Surprisingly, the one-part mortars gained lower water absorption and VPV, indicating a more densified microstructure in comparison to the normal mortar specimens after 28 days. However, after 56 days, the water absorption and VPV for the one-part mortars was 3.73% and 6.51% respectively, higher than those of the normal mortars. A higher porosity suggested by higher water absorption and VPV usually leads to lower compressive strength at later curing ages [40]. Hence, the 56-day results are in line with the mechanical strength, whereas the reduced 28-day compressive strength but lower water absorption and VPV for one-part mortars indicates that some other factors such as the loading capacity of the binding gels, any defects and/or precipitations may adversely influence the overall results [41].

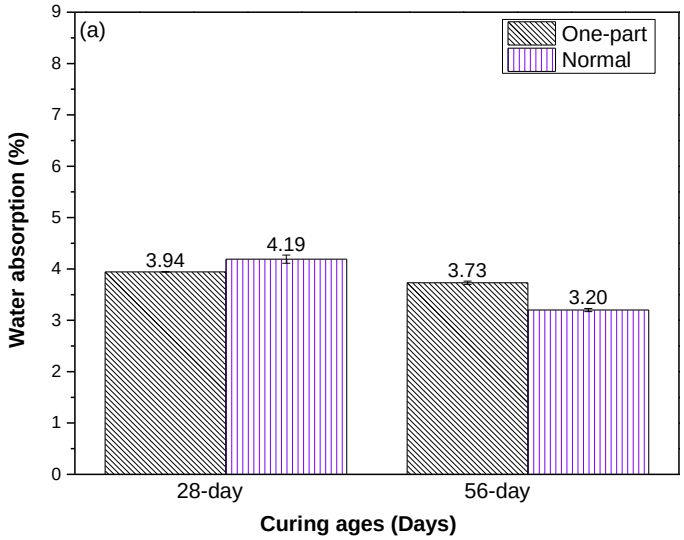

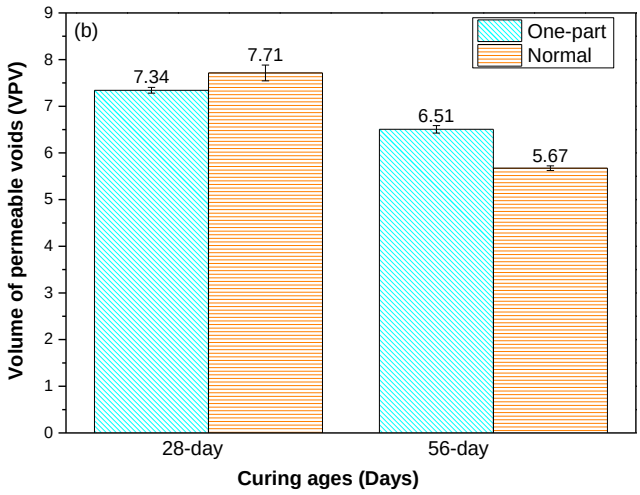

Fig. 9. Water absorption (a) and volume of permeable voids (b) of the two AAS mortar specimens after 28 days and 56 days of curing.

Different pore-size distributions for nanopores obtained from the nitrogen absorption test are shown in Fig. 10. Pores smaller than 50 nm in diameter can be categorized as gel pores, indicating the presence of alkali-activated gel products, such as C-A-S-H gels [42]. It seems that one-part mixed mortars had a lower volume of mesopores (less than 50 nm) compared to the normal peers, which suggests reduced degree of alkali activation and hence fewer C-A-S-H gels as compared to the normal AAS counterpart [21]. This was also evidenced by the lower surface area of the one-part specimens, which was only 3.788 m^2/g compared to 4.268 m^2/g for the normal peer. Fewer C-A-S-H gels would then result in lower compressive strength as the C-A-S-H gels are the main strength contributor to the AAS systems, in line with the compressive strength as shown in Fig. 7. Providing the higher water absorption and VPV (Fig.

9) but lower volume of mesopores in the one-part mortar specimens (Fig. 10), it can be inferred that this type of specimens had a greater amount of harmful pores (50-200 nm) and/or more-harmful pores (>200 nm) [43]. As a result, one-part specimens might have a poorer durability performance in comparison to the normal AAS specimens, which needs further investigations.

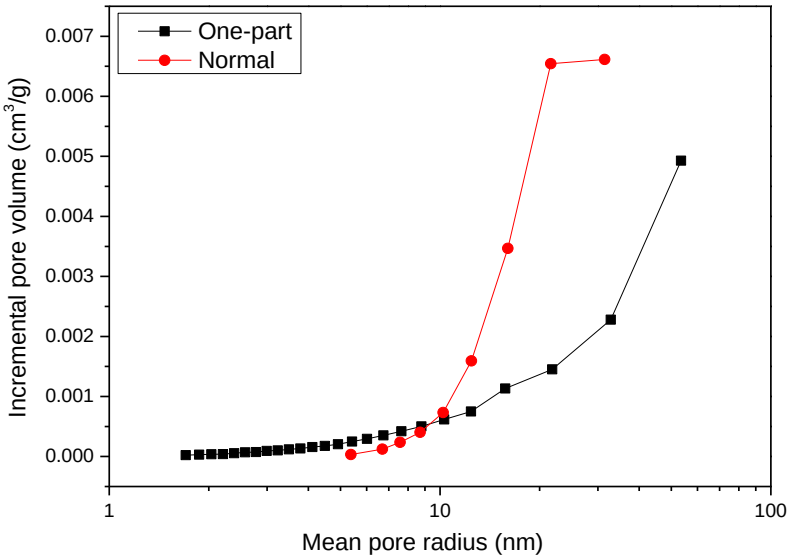

Fig. 10. Pore volume distribution of the one-part AAS and normal mortars after 56 days of curing.

3.3. Mineralogical and microstructural analysis

3.3.1. TGA/DTG

The relative gel content in the one-part and normal AAS pastes can be reflected by TGA and DTG curves, as shown in Fig. 11(a) and (b). For AAS binders, there are three stages of mass changes in TGA curves: i) the first stage up to 300 ℃ is assigned to the mass loss of free and bound water from C-A-S-H gels [44]; ii) the second stage from 300-710 ℃ is mainly attributed to chemically-bonded water loss and dehydroxylation of hydrotalcite-like phases [6, 45], loss of CO_2 from vaterite [46] or decomposition of calcite between 670 and 710 ℃ [47]; iii) the third stage above 710 ℃ is influenced by the decomposition of other calcite [46] and transitions of C-S-H and/or C-(A)-S-H to some crystalline phases [48]. The mass loss during the first stage can be used to quantify the degree of hydration since it is closely associated with the C-(A)-S-H gels. Specifically, the corresponding total mass loss within ‘Stage 1’ was 7.4% and 10.0% for the one-part and normal AAS pastes respectively. Thus, it shows that the former had fewer C-A-S-H gels than that of the normal mortar, corresponding well with the nitrogen adsorption

test results. Moreover, the total mass loss was 12.8% and 15.9% respectively, suggesting that the geopolymerisation process of one-part paste was not as complete as the normal counterpart.

For DTG, the decreased intensity of the endothermic peak assigned to the dehydration of C-(A)-S-H in the one-part AAS paste compared to the normal paste also suggests that the amount of C-(A)-S-H gel in the former was less. Moreover, the lower temperature marked as '1' at around 90 ℃ than that of the normal paste (denoted as '1'' at around 100 ℃) indicates a more densified structure of C-(A)-S-H in the normal AAS paste. Therefore, it seems that one-part mixing not only led to reduced amount of the main hydration products due in large part to the limited dissolution of GBFS, but may also negatively influence the polycondensation process and the resultant microstructures of the C-(A)-S-H gels. This is reasonable because for the one-part mixed specimens, the amount of available Al is less owing to the delayed dissolution of GBFS (the sole source of Al) into the alkaline activator. Hence, the structure of the binder was relatively weaker compared to the normal paste with higher amount of available alumina [49]. Besides, the weak shoulder at 220-230 ℃ and the small mass loss between 350 and 400 ℃, highlighted as '2' in the XRD pattern of the normal AAS paste, can be assigned to the presence of hydrotalcite-like phases [50, 51]. Thus, it is concluded that the one-part sample contained no hydrotalcite-like phases. This result corresponds well with other results implying that high-temperature or subzero temperature (-5, -10 and even -20 ℃) would all lead to the absence of hydrotalcite phase because when the temperature is too high or too low, the depolymerisation and polycondensation process would be adversely affected [14, 18, 21, 30]. In this study, the temperature of the one-part mixing is too high (Fig. 3), as mentioned earlier to explain the prolonged setting time, thus delaying the subsequent reaction process. In comparison, room temperature (23 ℃) or 0 ℃ could result in the formation of hydrotalcite [14, 20].

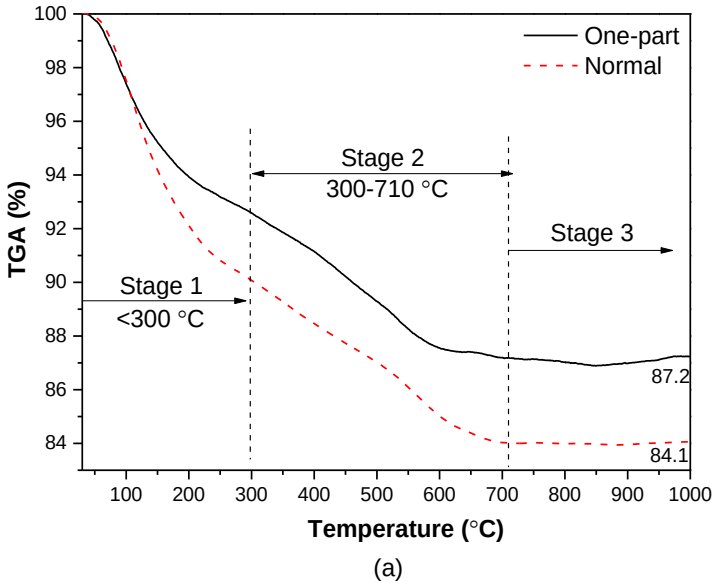

382

383

384 **Fig. 11.** (a) Thermogravimetric analysis (TGA); (b) differential thermogravimetry analysis
385 (DTG) of the one-part and normal AAS paste samples after 56 days of curing.

386

387 **3.3.2. XRD results**

388 According to the XRD patterns in Fig. 12, the similar broad peaks at around 29° 2θ for the
389 two AAS mixes can be assigned to the main hydration product, namely C-(A)-S-H gels, which
390 is in agreement with other studies [14, 46, 52]. Besides, the relative intensity of this peak for
391 the one-part specimen is lower compared to that for the normal specimen, implying that one-
392 part mixing led to the less formation hydration products, consistent with the TG/DTG results
393 and the lower compressive strength after 56 days of curing (shown in Fig. 7). In addition,
394 normal specimens also displayed some typical peaks that belong to hydrotalcite

($Mg_6Al_2CO_3(OH)_{16}\cdot 4H_2O$), indicating that there was some hydrotalcite formed in the normal specimens after 56 days. The formation of hydrotalcite often occurs when the content of MgO is more than 5 wt.% (as shown in Table 1) [20], corresponding well with the DTG curve as shown in Fig. 11(b). In addition, there are some traces of calcite evidenced by the two small diffraction peaks, which could be due to the carbonation of C-(A)-S-H gels [53].

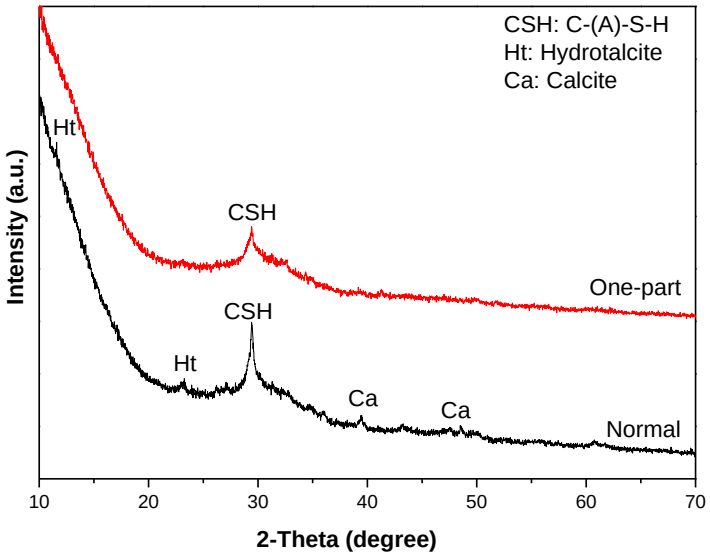

Fig. 12. X-ray diffraction patterns of the one-part and normal mixing AAS paste powders after 56 days of curing.

3.3.3. SEM/EDS

The morphology observations of the two types of AAS pastes and mortars are shown in Fig. 13 and Fig. 14, respectively. Based on Fig. 13, it can be seen that there are some crystals on the surface of the one-part AAS paste specimens which might be due to efflorescence. According to the EDS analysis, the crystals should be hydrated sodium carbonate ($Na_2CO_3\cdot nH_2O$) as the crystal is rich in Na, O and C [54], presented also in Fig. 13. In comparison, there is no efflorescence phenomenon for the normal AAS pastes. Considering that the efflorescence is highly dependent on the pores which act as a leaching channel [54, 55], this difference might be due to the fact that one-part specimens had more interconnected open pores since there was not enough C-A-S-H gels formed in the binding matrix. Moreover, the partial consumption of alkalis due to the local fast chemical reaction would lead to more available Na^+ ions in the pore solution. As a result, more free alkalis could travel through the porous systems to the surface of the samples. In contrast, normal AAS binders were more densified because of the physical compaction by different hydration products, as evidenced by the TG/DTG and XRD results. This result implies that one-part specimens are more prone to

efflorescence compared to its normal counterpart. Nonetheless, it should be noted that the amount of sodium carbonate is limited, since little signal of it was detected by DTG and XRD. Therefore, Fig. 13 does not lead to a firm conclusion that one-part AAS is subject to severe risk of efflorescence, rather it gives an indication that the efflorescence of one-part AAS might deserve further attention.

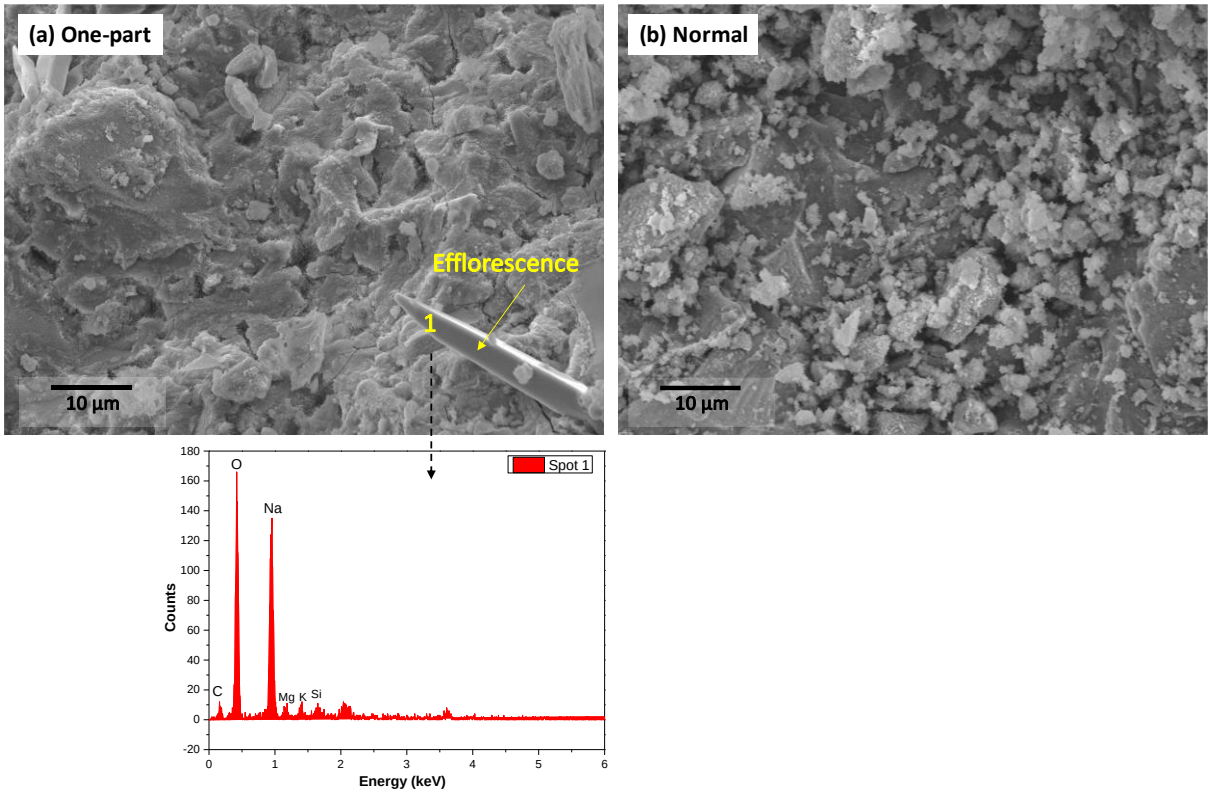

Fig. 13. SEM images (5000 × magnification) and EDS analysis of (a) one-part and (b) normal AAS paste specimens after 56 days of curing.

For mortar specimens, it can be seen that both two types of AAS mortars are compact including both paste and interfacial transition zone between the paste and sand particles, except some sharp crystals observed on the surface of the one-part mixed binding matrix. Therefore, the slightly lower mechanical strength might be associated with the presence of these small crystalline phases and/or some intrinsic defects as well as fewer C-(A)-S-H gels caused by the incomplete dissolution and reaction of GBFS particles in some regions of the binder because of the one-part mixing. Since paste samples were used in XRD and TGA tests, these crystals in ITZ region were not indicated in those tests. Polished samples with immersion of epoxy should be used to further investigate the properties of ITZ of AAS.

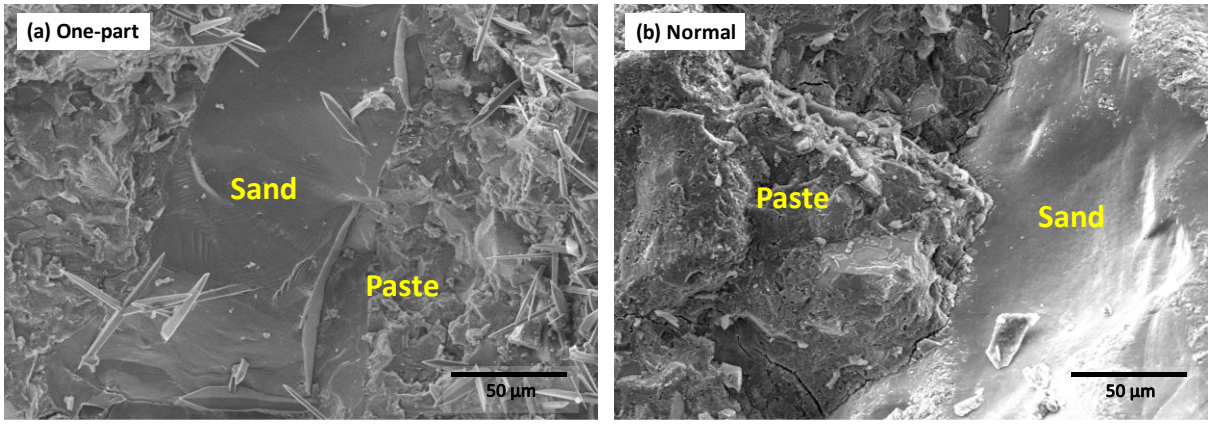

Fig. 14. SEM images (1500 × magnification) of (a) one-part and (b) normal AAS mortar specimens after 56 days of curing.

4. Conclusions

This study investigated both fresh and hardened properties of one-part and normal AAS binders activated by sodium metasilicate. According to the experimental results, several conclusions can be summarised as follows:

- Both the initial and final setting time was significantly prolonged for the one-part AAS binders compared to the normal counterpart due probably to the hard reaction shell formed under the condition of regional high rate of dissolution of GBFS owing to the rapid release of heat.
- One-part AAS mortars displayed slightly lower later-stage compressive strength than that of the normal counterparts but achieved similar values of compressive strength within about 7 days of curing. This can also be explained by considering the higher rate of dissolution of GBFS in some regions as evidenced by the early starting point of the acceleration stage in the heat evolution curves but overall a delayed and incomplete reaction of GBFS.
- One-part specimens had higher porosity evidenced by larger water absorption and VPV, but lower volume of mesopores, indicating that there should be more harmful pores which might affect the durability of these binders.
- The absence of hydrotalcite formed and fewer C-(A)-S-H gels for the one-part AAS binders correspond well with the delayed and incomplete hydration of GBFS suggested by other tests, which is closely associated with higher mixing temperature. Besides, one-part AAS binders seem to be more prone to efflorescence, evidenced by the crystals in the morphological and elemental analysis.

In general, it is feasible to use AAS binders given the similar fluidity and compressive strength as well as flexural strength. However, the much delayed hardening process, low degree of alkali activation of slags and high risks of efflorescence need extra focus.

Conflict of interest

The authors declare that they have no known competing financial interests or personal relationships that may influence the work reported in this paper.

Acknowledgements

This research work was financially supported by the National Natural Science Foundation of China (Grant Nos. 51878412, 51520105012, 51878413, and 51678368), the Shenzhen R&D Fund (Grant No. JCYJ20190808112019066), and the Guangdong Provincial Key Laboratory of Durability for Marine Civil Engineering (SZU) (Grant No. 2020B1212060074). Besides, Instrumental Analysis Center of Shenzhen University is also acknowledged.

References

[1] R.M. Andrew, Global CO2 emissions from cement production, Earth Syst. Sci. Data. Discuss. (2017).
[2] S. Zhang, A. Keulen, K. Arbi, G. Ye, Waste glass as partial mineral precursor in alkali-activated slag/fly ash system, Cement and Concrete Research 102 (2017) 29-40.
[3] S.-L. Zhang, X.-Q. Qi, S.-Y. Guo, J. Ren, J.-C. Chen, B. Chi, X.-C. Wang, Effect of a novel hybrid TiO_2-graphene composite on enhancing mechanical and durability characteristics of alkali-activated slag mortar, Construction and Building Materials 275 (2021) 122154.
[4] J. Ren, L. Zhang, R. San Nicolas, Degradation of alkali-activated slag/fly ash mortars under different aggressive acid conditions, Journal of materials in civil engineering (2020).
[5] J. Ren, S. Guo, J. Su, T. Zhao, J. Chen, S. Zhang, A novel TiO_2/Epoxy resin composited geopolymer with great durability in wetting-drying and phosphoric acid solution, Journal of Cleaner Production 227 (2019) 849-860.
[6] M.S. Kim, Y. Jun, C. Lee, J.E. Oh, Use of CaO as an activator for producing a price-competitive non-cement structural binder using ground granulated blast furnace slag, Cement and Concrete Research 54 (2013) 208-214.
[7] P. Sargent, P.N. Hughes, M. Rouainia, A new low carbon cementitious binder for stabilising weak ground conditions through deep soil mixing, Soils and Foundations 56(6) (2016) 1021-1034.
[8] C. Shi, B. Qu, J.L. Provis, Recent progress in low-carbon binders, Cement and Concrete Research 122 (2019) 227-250.
[9] T. Bakharev, J.G. Sanjayan, Y.B. Cheng, Sulfate attack on alkali-activated slag concrete, Cement and Concrete Research 32(2) (2002) 211-216.
[10] M. Albitar, M.M. Ali, P. Visintin, M. Drechsler, Durability evaluation of geopolymer and conventional concretes, Construction and Building Materials 136 (2017) 374-385.

[11] J. Ren, L. Zhang, R. San Nicolas, Degradation process of alkali-activated slag/fly ash and Portland cement-based pastes exposed to phosphoric acid, Construction and Building Materials 232 (2020) 117209.
[12] D.L. Kong, J.G. Sanjayan, Effect of elevated temperatures on geopolymer paste, mortar and concrete, Cement and concrete research 40(2) (2010) 334-339.
[13] A. Adam, Strength and durability properties of alkali activated slag and fly ash-based geopolymer concrete, School of Civil, Environmental and Chemical Engineering, RMIT University, 2009.
[14] M. Almakhadmeh, A.M. Soliman, Effects of mixing water temperatures on properties of one-part alkali-activated slag paste, Construction and Building Materials 266 (2021) 121030.
[15] W. Chen, R. Peng, C. Straub, B. Yuan, Promoting the performance of one-part alkali-activated slag using fine lead-zinc mine tailings, Construction and Building Materials 236 (2020) 117745.
[16] B. Yang, J.G. Jang, Environmentally benign production of one-part alkali-activated slag with calcined oyster shell as an activator, Construction and Building Materials 257 (2020) 119552.
[17] T. Luukkonen, Z. Abdollahnejad, J. Yliniemi, P. Kinnunen, M. Illikainen, One-part alkali-activated materials: A review, Cement and Concrete Research 103 (2018) 21-34.
[18] K. Wang, P.N. Lemougna, Q. Tang, W. Li, Y. He, X. Cui, Low temperature depolymerization and polycondensation of a slag-based inorganic polymer, Ceramics International 43(12) (2017) 9067-9076.
[19] Y.-m. Gu, Y.-h. Fang, D. You, Y.-f. Gong, C.-h. Zhu, Properties and microstructure of alkali-activated slag cement cured at below- and about-normal temperature, Construction and Building Materials 79 (2015) 1-8.
[20] T. Luukkonen, Z. Abdollahnejad, J. Yliniemi, P. Kinnunen, M. Illikainen, Comparison of alkali and silica sources in one-part alkali-activated blast furnace slag mortar, Journal of Cleaner Production 187 (2018) 171-179.
[21] A. Alzaza, K. Ohenoja, M. Illikainen, One-part alkali-activated blast furnace slag for sustainable construction at subzero temperatures, Construction and Building Materials 276 (2021) 122026.
[22] B. Nematollahi, J. Sanjayan, F.U.A. Shaikh, Synthesis of heat and ambient cured one-part geopolymer mixes with different grades of sodium silicate, Ceramics International 41(4) (2015) 5696-5704.
[23] M.X. Peng, Z.H. Wang, S.H. Shen, Q.G. Xiao, Synthesis, characterization and mechanisms of one-part geopolymeric cement by calcining low-quality kaolin with alkali, Materials and Structures 48(3) (2015) 699-708.
[24] J. Ren, H. Sun, K. Cao, Z. Ren, B. Zhou, W. Wu, F. Xing, Effects of natural seawater mixing on the properties of alkali-activated slag binders, Construction and Building Materials 294 (2021) 123601.
[25] J. Ren, S. Guo, T. Zhao, J. Chen, R. San Nicolas, L. Zhang, Constructing a novel nano-TiO_2/Epoxy resin composite and its application in alkali-activated slag/fly ash pastes, Construction and Building Materials 232 (2020) 117218.
[26] B. Yuan, Q.L. Yu, H.J.H. Brouwers, Time-dependent characterization of Na2CO3 activated slag, Cement and Concrete Composites 84 (2017) 188-197.
[27] I. Ismail, S.A. Bernal, J.L. Provis, S. Hamdan, J.S. van Deventer, Drying-induced changes in the structure of alkali-activated pastes, Journal of Materials Science 48(9) (2013) 3566-3577.
[28] J. Xing, Y. Zhao, J. Qiu, X. Sun, Microstructural and Mechanical Properties of Alkali Activated Materials from Two Types of Blast Furnace Slags, Materials (Basel, Switzerland) 12(13) (2019).

[29] Z. Li, M. Nedeljković, B. Chen, G. Ye, Mitigating the autogenous shrinkage of alkali-activated slag by metakaolin, Cement and Concrete Research 122 (2019) 30-41.
[30] B.S. Gebregziabiher, R.J. Thomas, S. Peethamparan, Temperature and activator effect on early-age reaction kinetics of alkali-activated slag binders, Construction and Building Materials 113 (2016) 783-793.
[31] F. Matalkah, L. Xu, W. Wu, P. Soroushian, Mechanochemical synthesis of one-part alkali aluminosilicate hydraulic cement, Materials and Structures 50(1) (2016) 97.
[32] K.-H. Yang, J.-K. Song, A.F. Ashour, E.-T. Lee, Properties of cementless mortars activated by sodium silicate, Construction and Building Materials 22(9) (2008) 1981-1989.
[33] C. Liu, X. Yao, W. Zhang, Controlling the setting times of one-part alkali-activated slag by using honeycomb ceramics as carrier of sodium silicate activator, Construction and Building Materials 235 (2020) 117091.
[34] W. Almakhadmeh, A.M. Soliman, COMPARATIVE ANALYSIS OF REACTION KINEATICS OF ONE AND TWO PARTS ALKALI ACTIVATED SLAG, CSCE Annual Conference, Laval (Greater Montreal), 2019.
[35] Z. Li, T. Lu, X. Liang, H. Dong, G. Ye, Mechanisms of autogenous shrinkage of alkali-activated slag and fly ash pastes, Cement and Concrete Research 135 (2020) 106107.
[36] Gruskovnjak, A., Lothenbach, B., Holzer, L., Figi, R., Winnefeld, F., Hydration of alkali-activated slag: comparison with ordinary Portland cement, Advances in Cement Research (2006).
[37] B. Nematollahi, J. Sanjayan, Ambient temperature cured one-part engineered geopolymer composite: a sustainable alternative to engineered cementitious composite, 9th Rilem International Symposium on Fiber Reinforced Concrete, 2016.
[38] J.L. Provis, R.J. Myers, C.E. White, V. Rose, J.S. van Deventer, X-ray microtomography shows pore structure and tortuosity in alkali-activated binders, Cement and Concrete Research 42(6) (2012) 855-864.
[39] P. Perumal, H. Sreenivasan, T. Luukkonen, A.M. Kantola, V.-V. Telkki, P. Kinnunen, M. Illikainen, High strength one-part alkali-activated slag blends designed by particle packing optimization, Construction and Building Materials 299 (2021) 124004.
[40] M.A. Megat Johari, J.J. Brooks, S. Kabir, P. Rivard, Influence of supplementary cementitious materials on engineering properties of high strength concrete, Construction and Building Materials 25(5) (2011) 2639-2648.
[41] A. Younis, U. Ebead, P. Suraneni, A. Nanni, Fresh and hardened properties of seawater-mixed concrete, Construction and Building Materials 190(NOV.30) (2018) 276-286.
[42] Sindhunata, J.L. Provis, G.C. Lukey, H. Xu, J.S.J. van Deventer, Structural Evolution of Fly Ash Based Geopolymers in Alkaline Environments, Industrial & Engineering Chemistry Research 47(9) (2008) 2991-2999.
[43] M.-h. Zhang, H. Li, Pore structure and chloride permeability of concrete containing nano-particles for pavement, Construction and Building Materials 25(2) (2011) 608-616.
[44] D. Shi, Y. Yao, J. Ye, W. Zhang, Effects of seawater on mechanical properties, mineralogy and microstructure of calcium silicate slag-based alkali-activated materials, Construction and Building Materials 212 (2019) 569-577.
[45] N. Mobasher, S.A. Bernal, J.L. Provis, Structural evolution of an alkali sulfate activated slag cement, Journal of Nuclear Materials 468 (2016) 97-104.
[46] U. De Filippis, E. Prud'homme, S. Meille, Relation between activator ratio, hydration products and mechanical properties of alkali-activated slag, Construction and Building Materials 266 (2021) 120940.
[47] N. Yang, W. Yue, The Handbook of Inorganic Metalloid Materials Atlas (in Chinese), Wuhan University of Technology Press2000.

[48] N.K. Lee, K.T. Koh, G.H. An, G.S. Ryu, Influence of binder composition on the gel structure in alkali activated fly ash/slag pastes exposed to elevated temperatures, Ceramics International 43(2) (2017) 2471-2480.
[49] E. Najafi Kani, A. Allahverdi, J.L. Provis, Efflorescence control in geopolymer binders based on natural pozzolan, Cement and Concrete Composites 34(1) (2012) 25-33.
[50] O. Burciaga-Díaz, I. Betancourt-Castillo, Characterization of novel blast-furnace slag cement pastes and mortars activated with a reactive mixture of MgO-NaOH, Cement and Concrete Research 105 (2018) 54-63.
[51] M. Ben Haha, G. Le Saout, F. Winnefeld, B. Lothenbach, Influence of activator type on hydration kinetics, hydrate assemblage and microstructural development of alkali activated blast-furnace slags, Cement and Concrete Research 41(3) (2011) 301-310.
[52] J. Zhang, C. Shi, Z. Zhang, Z. Ou, Durability of alkali-activated materials in aggressive environments: A review on recent studies, Construction and Building Materials 152 (2017) 598-613.
[53] R.J. Myers, E. L'Hôpital, J.L. Provis, B. Lothenbach, Effect of temperature and aluminium on calcium (alumino)silicate hydrate chemistry under equilibrium conditions, Cement and Concrete Research 68 (2015) 83-93.
[54] Z. Zhang, J.L. Provis, A. Reid, H. Wang, Fly ash-based geopolymers: the relationship between composition, pore structure and efflorescence, Cement and Concrete Research 64 (2014) 30-41.
[55] P. Zhang, Q.-F. Li, Durability of high performance concrete composites containing silica fume, Proceedings of the Institution of Mechanical Engineers, Part L: Journal of Materials Design and Applications 227 (2013) 343-349.